UNIVERSITY OF BIRMINGHAM

Influence of temperature and pressure on surface modified Pd-Cu alloy foils for hydrogen purification applications

Al-Mufachi, Naser; Steinberger-Wilckens, Robert

[Link to publication on Research at Birmingham portal](#)

Accepted Manuscript

Influence of temperature and pressure on surface modified Pd-Cu alloy foils for hydrogen purification applications

Naser A. Al-Mufachi, Robert Steinberger-Wilckens

Please cite this article as: Naser A. Al-Mufachi, Robert Steinberger-Wilckens , Influence of temperature and pressure on surface modified Pd-Cu alloy foils for hydrogen purification applications. The address for the corresponding author was captured as affiliation for all authors. Please check if appropriate. Tsf(2017), doi:10.1016/j.tsf.2017.11.032

Influence of temperature and pressure on surface modified Pd-Cu alloy foils for hydrogen purification applications

Naser A. Al-Mufachi* and Robert Steinberger-Wilckens

Centre for Fuel Cell and Hydrogen Research, School of Chemical Engineering, University of Birmingham, Edgbaston B15 2TT, UK

*Corresponding author:
E-mail address: n.a.al-mufachi@bham.ac.uk
Tel: + 44 121 414 5081

Abstract

The surface of as-received $Pd_{60}Cu_{40}$ wt% foil samples was modified by depositing a Pd thin film onto one side. X-ray diffraction analysis revealed that the as-received $Pd_{60}Cu_{40}$ wt% foil contained only the disordered face centred cubic (FCC) phase. Three different Pd thin film thicknesses (100, 800 and 1,400 nm) were deposited using magnetron sputtering onto the as-received $Pd_{60}Cu_{40}$ wt% foil to produce the surface modified foil samples. X-ray diffraction and X-ray photoelectron spectroscopy analysis of these samples showed a strong indication that Cu interdiffusion occurred between the bulk Pd-Cu foil and Pd thin film during the deposition process.

For the first time, variable temperature X-ray diffraction analysis has been performed on the surface modified foil samples between 30 and 700 °C under 100 and 445 kPa of hydrogen pressure in order to investigate the effects of these conditions on Cu interdiffusion. In general, it was found that under 445 kPa of hydrogen pressure the palladium hydride (β-PdH) phase present in the thin film is stable up to higher temperatures (225 °C) than under 100 kPa of hydrogen pressure (150 to 175 °C). In all cases, it was observed that the interstitial solid solution (α-PdH) phase present within the thin film is stable under a significantly narrower temperature range under 445 kPa of hydrogen pressure when compared to 100 kPa.

Keywords

Pd-Cu alloy
Foil characterisation
Pd thin film
Hydrogen purification
Interdiffusion
Alloy foils

1   Introduction

Today, a majority of the commercially available hydrogen gas on the market is produced by steam methane reforming [1]. With recent concerns over climate change and peak oil, there has been a growing demand for alternative green energy. This has resulted in the rising popularity of the polymer electrolyte fuel cells (PEFC) which utilise ultra-pure hydrogen (99.999%) to produce electricity. As expected, there is now an increasing demand for high purity hydrogen [2, 3]. Palladium-based dense alloy membranes are commonly used for hydrogen purification applications as they possess high catalytic activity for dissociation of hydrogen gas molecules, excellent hydrogen permeability, high selectivity and good durability [4-8]. Of particular interest is the Pd-Cu alloy system since the reduced Pd content yields a cheaper material and the Pd-rich Pd-Cu FCC phase demonstrates improved tolerance to H_2S contamination when compared to similar competing commercial membranes, for example the Pd-Ag alloy type [7, 9-14].

Fig. 1 depicts the Pd-Cu phase diagram, which reveals that below 450 °C the composition of $Pd_{60}Cu_{40}$ wt% contains an ordered body centred cubic (BCC) crystal structure displaying a CsCl-type lattice [15]. For this binary alloy system, the $Pd_{60}Cu_{40}$ wt% composition has been shown to exhibit the highest hydrogen permeability [4, 9, 10, 14, 16, 17]. As demonstrated in Fig. 1, a deviation equal to or greater than 3 wt% from this optimal composition can have the effect of drastically reducing the hydrogen permeability by a minimum of 50% [18]. This study is focussed on $Pd_{60}Cu_{40}$ wt% alloy foils, therefore any further reference to Pd-Cu foils in this work will be of this composition, unless otherwise stated.
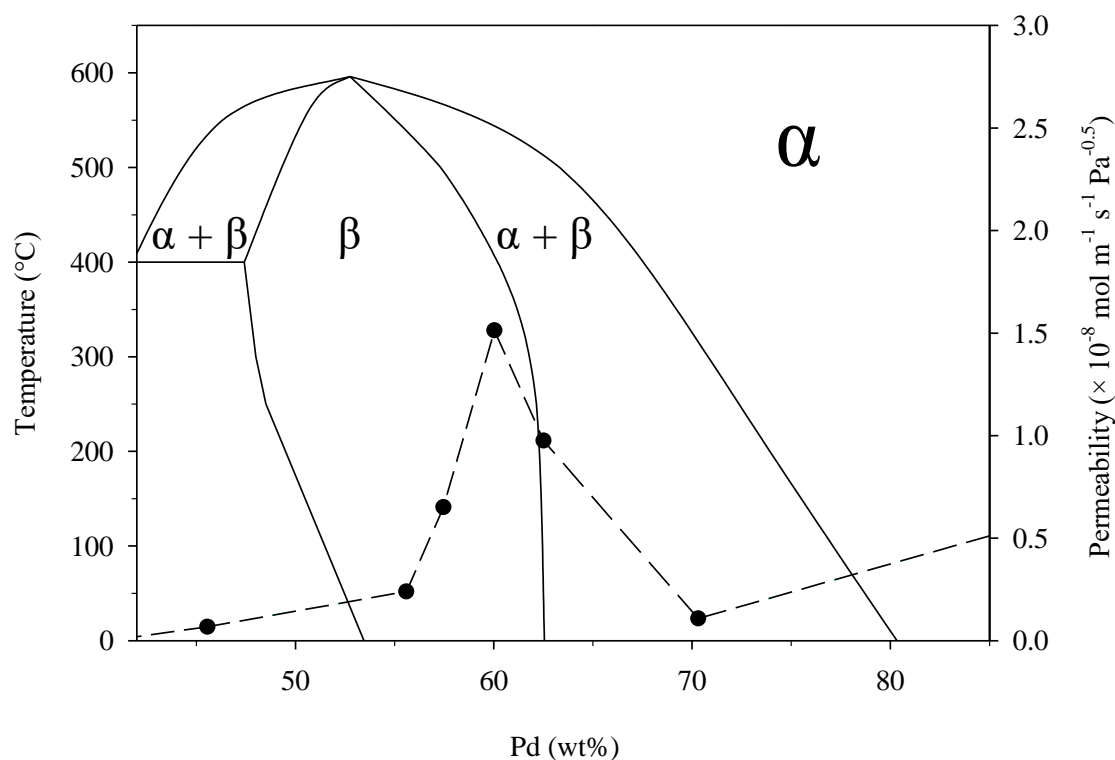
Fig. 1 The Pd-Cu phase diagram showing the FCC (α), BCC (β) and mixed α + β phase regions [19] which has been recreated from literature [15, 20] and includes a hydrogen permeability dashed line curve plot as a function of Pd content at 350 °C sourced from published data [17].

Within the Pd-Cu system, hydrogen diffusivity of the ordered BCC phase is two orders of magnitude higher than the counterpart disordered FCC phase [16, 17, 21, 22]. For the $Pd_{60}Cu_{40}$ wt% composition, the FCC phase emerges above 450 °C to coexist with the BCC phase. However, only the FCC phase is present and stable above 600 °C. Interestingly, the Pd-rich Pd-Cu FCC phase possesses relatively higher hydrogen solubility [23-25] and an increased tolerance to H_2S contamination in comparison to the BCC phase [12, 14].

It was previously reported [26] that depositing a Pd thin film onto one side of an FCC $Pd_{60}Cu_{40}$ wt% alloy foil membrane had the effect of increasing hydrogen permeability when the coated surface was positioned on the relatively high hydrogen pressure feed side during rig testing. This improvement in hydrogen permeability has been attributed to the presence of the Pd-rich Pd-Cu FCC phase which is formed as a result of Cu interdiffusing out of the bulk $Pd_{60}Cu_{40}$ wt% foil membrane and into the Pd thin film. Understanding the influence of temperature and hydrogen pressure on the formation and stability of such a phase would be essential when attempting to optimise the performance of dense metal membranes. The aim of this work is to investigate the effects of temperature and hydrogen pressure on the interdiffusion process between $Pd_{60}Cu_{40}$ wt% foil and Pd thin film using a variety of characterisation techniques.

2   Experimental

3

2.1 Sample preparation

A 31.3 ± 0.8 μm thick cold rolled $Pd_{60}Cu_{40}$ wt% foil batch, supplied by Johnson Matthey Noble Metals (Royston, UK), was used in this study. Seven square (~25 mm^2) foil samples were cut from this as-received Pd-Cu foil batch and cleaned in acetone for 5 minutes using an ultrasonic bath.

2.2 Magnetron sputtering

The surface of the square Pd-Cu foil samples was modified by depositing a Pd thin film using a closed field unbalanced magnetron sputter ion plating (CFUBMSIP) system manufactured by Teer Coatings Ltd [27]. The Pd-Cu foil samples were mounted inside the sputtering system (evacuated to 10^{-7} kPa) and subjected to an ion cleaning process with Ar plasma prior to sputtering. The sputtering process utilises a Pd target (99.9% purity) which was sputter-coated onto the Pd-Cu foil samples at a target current of 1 A and an Ar flux of 25 standard cm^3 min^{-1}. Three different Pd deposition times were selected with the aim of producing Pd-Cu surface modified foil samples with varying Pd thin film thicknesses on one side.

In Table 1, the Pd-Cu foil samples are categorised into four types. Foil A was not Pd sputter-coated and remained in the as-received state. The letters B, C and D indicate that the surface modified foil samples have been Pd sputter-coated for 50, 1,000 and 1,800 seconds, respectively. A set of three surface modified foil samples were prepared with each deposition run.

In addition, a glass slide was Pd sputter-coated with each sample type whereby a section of the glass surface was protected with Kapton tape. Tape removal revealed the non-coated surface of the glass slide which produced a step from which the Pd film thickness could be determined. An Ambios XP-200 Stylus surface profilometer with a scanning speed of 0.1 mm s^{-1} using a 2 mg tip force was used to accurately measure the thickness of the Pd thin film. Table 1 shows the Pd thin film thicknesses for each foil type obtained using profilometry measurements performed on the respective Pd coated glass slides.

4

Table 1 Summary of samples used in this study.

Samples	Pd deposition time (s)	Pd thin film thickness (nm)
Foil A	Not coated	-
Foils B1, B2, B3	50	~100
Foils C1, C2, C3	1,000	~800
Foils D1, D2, D3	1,800	~1,400

2.3 X-ray diffraction analysis

Ex-situ X-ray diffraction (XRD) patterns were obtained for both surfaces of the foils under ambient conditions. The XRD patterns contain information on both the Pd thin film in the Pd-Cu foil samples, in addition to the underlying bulk Pd-Cu foil all depending on the X-ray penetration depth. The XRD analyses were carried out on a Bruker D8-Advance diffractometer using monochromatic CuK$_{\alpha 1}$ radiation ($\lambda = 1.54056$ Å).

In-situ variable temperature XRD (VTXRD) was performed on the surface modified foil samples using an Anton Paar XRK 900 pressure cell in order to observe any phase transformations and interdiffusion between the Pd thin film and bulk Pd-Cu foil. VTXRD studies were performed on Foils B2, C2 and D2 under 445 kPa of flowing hydrogen. Additionally, VTXRD studies were performed on Foils B3, C3 and D3 under 100 kPa of flowing hydrogen. VTXRD scans were conducted isothermally before heating to the next temperature set point. The temperature ramp rate used for all VTXRD experiments was 2.4 °C min^{-1} heating from 30 to 700 °C and then cooled back to 30 °C at approximately 5 °C min^{-1}.

2.4 Scanning electron microscopy/Energy dispersive spectroscopy analysis

A Joel 6060 microscope was used to perform scanning electron microscopy (SEM) in secondary electron imaging mode and energy dispersive spectroscopy (EDS) was conducted using INCA EDAX software. SEM and EDS was used to determine the composition of the as-received foil and any compositional variation in the samples prior to VTXRD analysis.

2.5 X-ray photoelectron spectroscopy

X-ray photoelectron spectroscopy (XPS) depth profiling was performed on the as-deposited Foils B1, C1 and D1 to examine any interdiffusion occurring between the Pd thin film and bulk Pd-Cu foil during the Pd deposition process. Futhermore, XPS depth profiling was carried out on Foils B2, B3, C2, C3, D2 and D3 following VTXRD analysis in order to investigate the effects of high temperatures and hydrogen pressures on surface and subsurface composition.

Depth profile analysis was performed with a Thermo K-Alpha XPS Spectrometer with a monochromated K-Alpha source fitted with a MAGCIS ion gun. The charge compensation was active during measurements. A monatomic Ar gun mode was used for the etch cycles with a 2 keV ion beam. The scan area was 4 mm^2 and a reference etching rate of 0.21 nm s^{-1} based on a Ta$_2$O$_5$ standard was used for etch depth estimation. A suitable etch

5

cycle and etch depth was chosen according to the Pd thin film thickness being analysed. Pd thin films with relatively smaller thicknesses had a shorter etch cycle compared to relatively thicker Pd thin films in order to obtain higher detail and resolution of the interface region.

3   Results and discussion

3.1   Pre-VTXRD foil characterisation

In the as-received state, the nominal composition of the foil used in this study was stated as $Pd_{60}Cu_{40}$ wt%. According to the Pd-Cu phase diagram (Fig. 1), the $Pd_{60}Cu_{40}$ wt% composition contains a CsCl-type ordered BCC equilibrium phase below 450 °C. Fig. 2(a) shows a representative ex-situ XRD pattern of Foil A. The analysis indicates the presence of the disordered FCC structure which is likely due to the alloy being quenched from the high temperature FCC phase during the melting process.
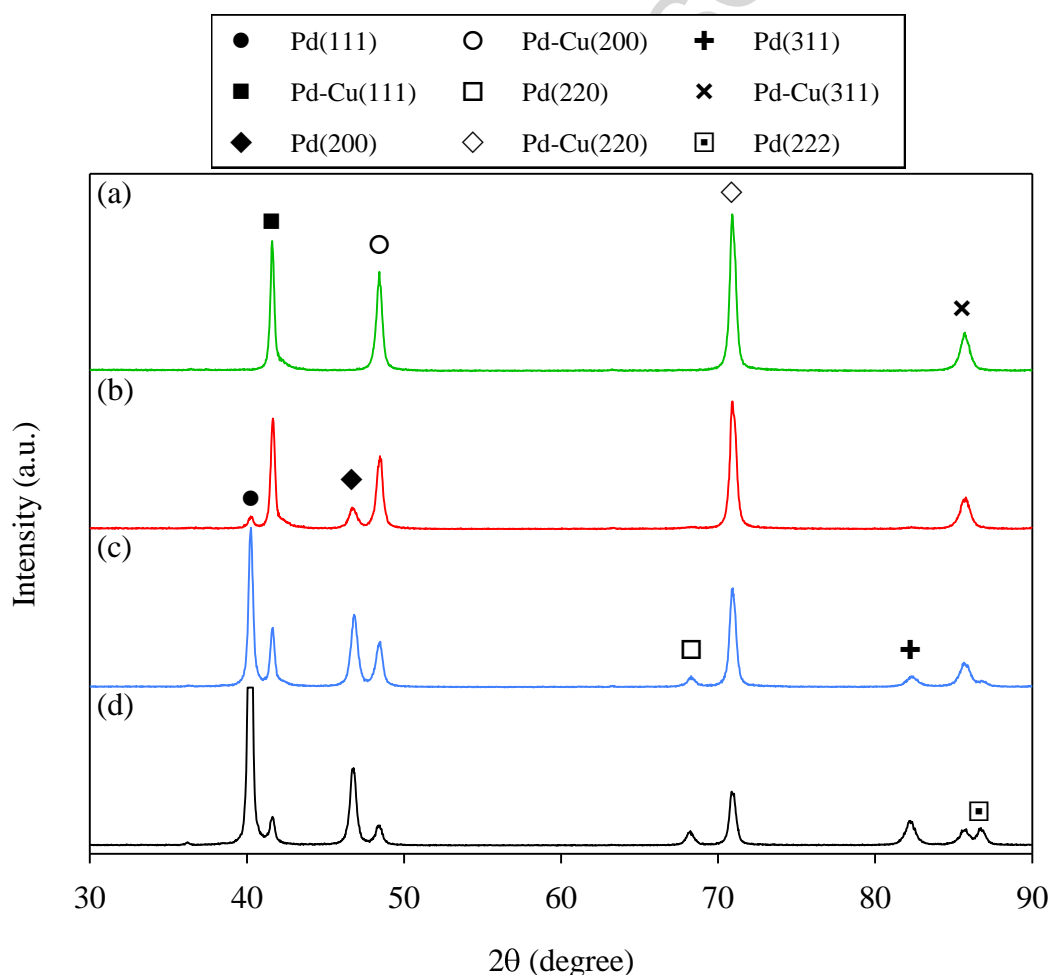
Fig. 2 Representative ex-situ XRD patterns acquired for (a) Foil A and the Pd sputter-coated surfaces of (b) Foils B1 to 3, (c) C1 to 3 and (d) D1 to 3 in the as-deposited state. The Pd diffraction peaks shown in patterns (b), (c) and (d) indicate the presence of the Pd thin film.

According to Vegard's law (Eq. (1)), there is a linear relationship between crystal lattice parameter (a) and concentration of constituent alloying elements (x_{Pd}) in at% [28].

Eq. (1) has been derived elsewhere [19] and has been used in this study to determine crystal lattice parameter of all foil samples.

$$a = (2.7522 \times 10^{-3})x_{Pd} + 3.6226 \tag{1}$$

Using XRD data analysis, the lattice parameter for both sides (Side (a) and Side (b)) of Foil A in the as-received state was determined. The lattice parameters were calculated as 3.759 and 3.754 Å for Side (a) and Side (b), respectively. These lattice parameters are comparable to published values of the same FCC phase composition which range between 3.75 and 3.764 Å [16, 29-33].

In Table 2, the calculated lattice parameters have been used to determine the associated FCC phase compositions and compared with the EDS chemical analysis results. It is apparent that Side (a) has a different FCC phase composition to that of Side (b) indicating that the Pd-Cu foil has compositional inhomogeneity. This observation is corroborated well by the EDS results despite the compositions obtained from either technique not matching exactly. It should be noted that the EDS analysis sampled information from the Pd-Cu foil over a relatively smaller area (~150 μm^2) compared to XRD which scans and collects information from the entire foil surface (~25 mm^2). Hence, the compositions obtained using XRD analysis are considered to be more accurate and therefore it can be said that the average FCC phase composition for the Pd-Cu foil in the as-received state is $Pd_{61.3}Cu_{38.7}$ wt%.

Table 2 A summary of the FCC phase compositions (wt%) determined using XRD and EDS for both the as-received Pd-Cu foil used in this study.

Surface	XRD	EDS
Side (a)	$Pd_{62.0}Cu_{38.0}$	$Pd_{60.8}Cu_{39.2}$
Side (b)	$Pd_{60.6}Cu_{39.4}$	$Pd_{57.6}Cu_{42.4}$

As outlined in Table 1, Foils B1, B2 and B3 were prepared by sputtering Pd onto one side of an as-received Pd-Cu foil for 50 seconds. The thickness of the Pd thin film was determined using profilometry to be 95.5 ± 0.1 nm thick.

Fig. 2(b) illustrates a representative XRD pattern for the Pd sputter-coated side of Foils B1, B2 and B3 in the as-deposited state. The presence of the Pd thin film is indicated by the Pd(111), (200), (220), (311) and (400) diffraction peaks. A noticeable feature of Fig. 2(b) is the peak asymmetry evident in these diffraction peaks. With peak asymmetry, the diffraction peaks themselves are made up of smaller individual diffraction sub-peaks positioned at different scattering angles. Yet the XRD pattern combines the individual peaks into one asymmetric diffraction peak.

The Pd(111) diffraction peak from Fig. 2(b) is shown in greater detail in Fig. 3. Asymmetry in this peak is observed on the right hand side spreading over a range of higher scattering angles. An increase in scattering angle is caused by a decrease in inter-planar distance and consequently a reduction in the lattice parameter. As expected, the Pd-Cu FCC crystal structure contracts with increasing Cu content. This may suggest that interdiffusion of Cu atoms from the Pd-Cu foil into the Pd thin film takes place during the sputtering process producing an interface region that exhibits a range of Pd-Cu compositions.

7

From points A, B, C, D and E in Fig. 3, the corresponding compositions were determined and compiled in Table 3. It should be noted that XRD data points were acquired every 0.028° 2θ in each pattern and it is assumed that this step size is sufficient for a good first approximation. Point A is highlighted with a green dashed line to indicate the 2θ position of the pure Pd(111) diffraction peak.
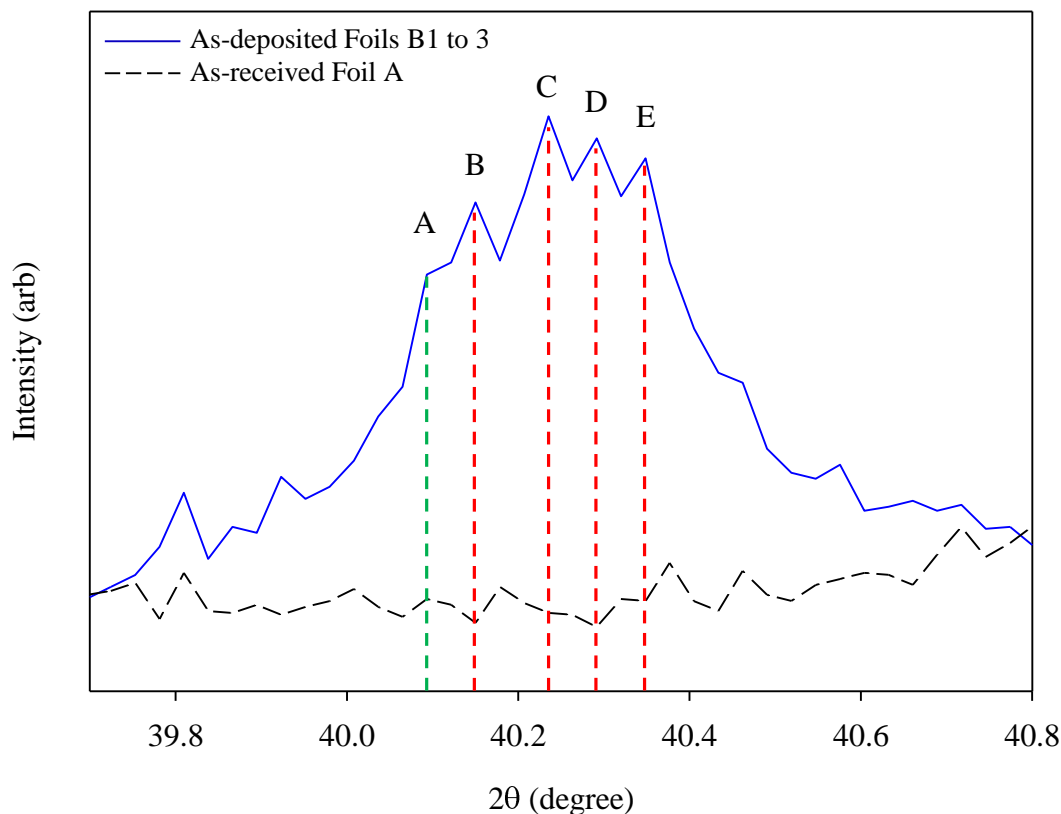
Fig. 3 Magnification of the Pd(111) diffraction peak shown in Fig. 2(b) featuring an XRD pattern of the uncoated as-received Foil A for comparison.

Table 3 Compositions determined for points A to E in Fig. 3.

	Scattering angle, 2θ (degree)	Composition (wt%)
A	40.09	$Pd_{100}Cu_0$
B	40.15	$Pd_{97.6}Cu_{2.4}$
C	40.24	$Pd_{95.8}Cu_{4.2}$
D	40.29	$Pd_{94.6}Cu_{5.4}$
E	40.35	$Pd_{93.4}Cu_{6.6}$

Using the scattering angles for the most intense peaks corresponding to each Pd-Cu(*hkl*) diffraction plane (for example point C in Fig. 3), the composition of the Pd thin film was calculated to be $Pd_{95.8}Cu_{4.2}$ wt%.

It is well known that substantial interdiffusion can happen between bimetallic interfaces in bulk metals and alloys at the Tammann temperature [34]. The Tammann temperature is defined as the point at which atoms within a bulk solid are sufficiently mobile for bulk-to-surface diffusion and is estimated to be half of the melting point (MP) in degrees Kelvin. Therefore, for the Pd-Cu system the Tammann temperature is expected to range

between 679 K/326 °C (MP$_{Cu}$) and 914 K/641 °C (MP$_{Pd}$). It is also expected that the relatively lighter Cu atoms will be the most mobile specie when compared to the heavier Pd atoms. Several studies on this topic [35-40] have demonstrated that significant interdiffusion can transpire in Pd-Cu thin films produced with a range of deposition techniques including electrodeposition, thermal evaporation and magnetron sputtering. Furthermore, it has been reported that interdiffusion between Pd/Cu multilayers occurs at 120 °C and it is suspected that these polycrystalline thin films introduce a large grain boundary volume that enables interdiffusion at such low temperatures [40].

XPS depth profile analysis was performed on Foil B1 in the as-deposited state to observe the variation in Pd and Cu concentration as a function of etch depth which is shown in Fig. 4(a). An estimate for etch depth was determined from the etch time using an etching rate of 0.21 nm s^{-1} obtained from a Ta$_2$O$_5$ standard. According to Fig. 4(a), Foil B1 has a 75 nm thick pure Pd top layer beyond which resides an interdiffusion region. It should be pointed out that XPS depth profile analysis was carried out down to 200 nm and it is likely that the interdiffusion region continues further on which means that larger analysis depths are necessary to reach the underlying bulk Pd-Cu foil. Nevertheless, this provides proof that interdiffusion takes place between the deposited Pd thin film and bulk Pd-Cu foil throughout the deposition process. XPS scans were acquired at 25 nm increments, however, smaller increments may provide a much higher resolution and detail of the depth and extent of the interdiffusion region.

Despite the short deposition time of 50 seconds, it is still plausible that interdiffusion could occur between the Pd thin film and bulk Pd-Cu foil in Foil B1. It is likely that the sputtered Pd atoms achieve a sufficiently high enough kinetic energy as they accelerate towards the Pd-Cu foil to locally increase the surface temperature upon impact thus facilitating interdiffusion.
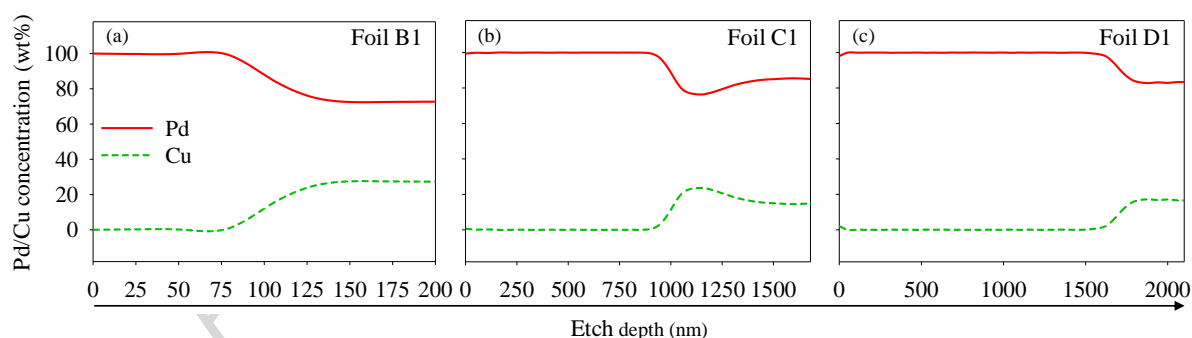
Fig. 4 XPS depth profile analysis of (a) Foils B1, (b) C1 and (c) D1 in the as-deposited state.

Profilometry of a glass slide that was simultaneously coated with Foils C1, C2 and C3 revealed a Pd film thickness of approximately 797.4 ± 0.2 nm.

Fig. 2(c) depicts a representative XRD pattern acquired from the Pd sputter-coated surface of Foils C1, C2 and C3. In the as-deposited state, Foils C1, C2 and C3 indicate the presence of a single FCC phase. The presence of the Pd thin film is clearly indicated by the Pd diffraction peaks. The relatively high intensity displayed by the low scattering angle

Pd(111) and Pd(200) diffraction peaks is due to the incident X-ray beam glancing the top surface of Foil C1, C2 and C3, collecting a majority of the information from the Pd thin film.

As the Pd thin film is deposited onto Foils C1, C2 and C3, growth proceeds and the Pd adsorbed atoms (adatoms) have the tendency to arrange themselves into the most densely packed plane as this configuration has the lowest free energy. The most densely packed plane for the FCC crystal structure is the (111) plane. The relatively high intensity Pd(111) diffraction peak shown in Fig. 2(c), indicates that the Pd adatoms have mainly assumed this arrangement.

Using the scattering angles associated with the Pd(hkl) diffraction peaks, the composition of the Pd thin film was calculated to be $Pd_{99.5}Cu_{0.5}$ wt% indicating that, although minute, there is evidence for interdiffusion of Cu atoms from the bulk Pd-Cu foil into the Pd thin film occurring during the Pd deposition process.

Fig. 4(b) displays the results of the XPS depth profile analysis performed on Foil C1. An XPS scan resolution of 50 nm was implemented during the analysis. The Cu concentration starts to increase at a rough depth of 890 nm and level off at 1,050 nm highlighting the beginning of the interdiffusion region giving further evidence that interdiffusion happens during the deposition process. At greater depths, a bottleneck region emerges emanating from the bulk Pd-Cu foil revealing that the Cu concentration declines and plateaus at around 1,500 nm which may be due to the residual effects of a phenomenon known as coring. In this instance, coring would cause the relatively lower melting point Cu atoms to diffuse towards the outer regions of the foil whereas the Pd atoms would concentrate around the inner region. In order to reach the original composition of the bulk Pd-Cu foil (~$Pd_{60}Cu_{40}$ wt%), it would likely be necessary to analyse to depths greater than 1,680 nm.

The glass slide routinely Pd sputter-coated alongside Foils D1, D2 and D3 was analysed using profilometry revealing a Pd thin film thickness of approximately $1,409.6 \pm 0.2$ nm.

The representative XRD pattern is illustrated in Fig. 2(d) for the Pd sputter-coated side of Foils D1, D2 and D3 in the as-deposited state, indicating the presence of only the FCC phase. The Pd(111) diffraction peak associated with the Pd thin film has the highest relative intensity giving evidence that the Pd adatoms are preferentially arranged in the most densely packed (111) plane. A Pd thin film composition of $Pd_{98.1}Cu_{1.9}$ wt% was determined using the scattering angles associated with the Pd(hkl) diffraction peaks demonstrating again that interdiffusion between the deposited film and the bulk Pd-Cu foil occur during the sputtering process.

The XPS depth profile analysis for Foil D1 is displayed in Fig. 4(c) which uses a 50 nm resolution. It is shown that the Cu concentration starts to rise at around a depth of 1,520 nm revealing the start of the interdiffusion region and plateaus at approximately 1,800 nm. It seems necessary to etch and analyse to greater depths in order to detect the bulk Pd-Cu foil present beneath the Pd thin film layer.

3.2 VTXRD foil analysis

VTXRD analysis was performed on Foils B2 and B3 between 30 and 700 °C to study the influence of temperature and hydrogen pressure on the interdiffusion of the Pd thin film with the bulk Pd-Cu foil.

Foil B2 was tested under 445 kPa of flowing hydrogen in order to emulate typical operating conditions of dense metal membranes. Fig. 5(a) is a contour plot of temperature against scattering angle. It is apparent from this plot that the Pd thin film forms the β-PdH phase at temperatures as low as 30 °C. This is shown by the β-PdH(111) diffraction peak located at $2\theta = 38.30°$. Hence, the Pd lattice parameter expands from 3.89 to 4.067 Å which is a 14.3% lattice volume expansion as a result of 445 kPa of hydrogen pressure. The β-PdH(111) diffraction peak shifts to $2\theta = 39.81°$ at 200 °C indicating the formation of the α-PdH phase as hydrogen is desorbed from the Pd thin film with increasing temperature. Due to hydrogen desorption, the lattice parameter contracts to 3.92 Å. This observation is expected since the enthalpy of hydride formation in Pd is exothermic [41].
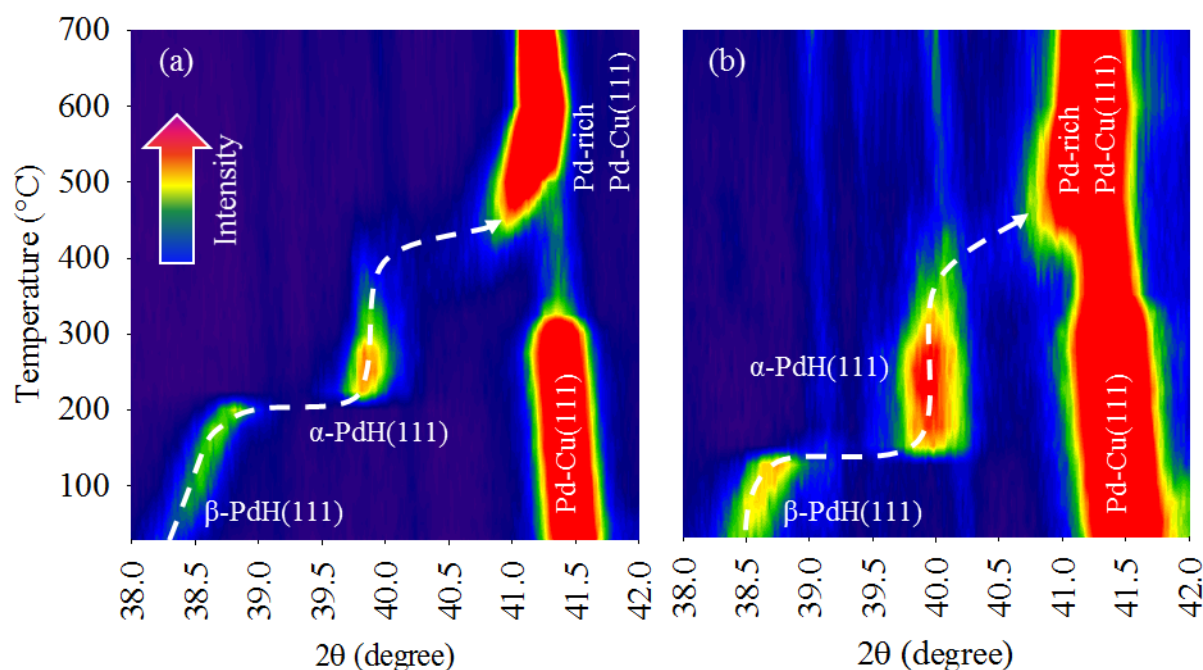

Fig. 5 VTXRD contour plots tracking the movement of the (a) PdH(111) diffraction peak from the Pd thin film of Foil B2 under 445 kPa of flowing hydrogen and (b) the PdH(111) diffraction peak from the Pd thin film of Foil B3 under 100 kPa of flowing hydrogen whilst heating between 30 and 700 °C.

The interdiffusion process takes place between 350 and 600 °C as shown by the movement of the α-PdH(111) diffraction peak to higher scattering angles. This peak shift is indicative of a decrease in interplanar distance and consequently lattice parameter as a result of the Cu concentration increasing in the Pd thin film. At temperatures above 600 °C interdiffusion stops as the α-PdH(111) diffraction peak eventually merges with the newly formed Pd-rich Pd-Cu(111) diffraction peak demonstrating that the Pd thin film has fully interdiffused with the bulk Pd-Cu foil.

Also, note that the Pd-Cu(111) diffraction peak attributed to the FCC phase present in the bulk Pd-Cu foil, drops in intensity between 325 and 500 °C. This means that the FCC content in the bulk Pd-Cu foil dramatically drops between these temperatures. According to Fig. 1, at a composition of $Pd_{60}Cu_{40}$ wt% the FCC phase is stable at 450 °C and above, but it has been previously observed that dissolved hydrogen has the profound effect of shifting the BCC | FCC + BCC phase boundary to higher Pd concentrations [16]. This would mean that

11

under 445 kPa of hydrogen pressure the FCC phase present in the bulk Pd-Cu foil is stable at higher temperatures, which in this case is 500 °C and above.

VTXRD was conducted on Foil B3 under 100 kPa of flowing hydrogen (Fig. 5(b)). Similar to Foil B2, the Pd thin film readily forms the β-PdH phase at 30 °C, however, the β-PdH(111) diffraction peak occurs at a relatively higher scattering angle, $2\theta = 38.53°$. This scattering angle signifies that the Pd lattice parameter has increased to 4.043 Å as a result of exposure to 100 kPa of hydrogen pressure causing a 12.3% lattice volume dilation. From this it is evident that 445 kPa of hydrogen pressure generates a larger lattice expansion in the Pd thin film compared to a pressure of 100 kPa.

Furthermore, Fig. 5(b) shows that at 150 °C the β-PdH(111) diffraction peak shifts to $2\theta = 39.98°$ indicating that hydrogen desorption in the Pd thin film occurs to form the α-PdH phase. According to the Pd-H pressure-composition-temperature (PCT) diagram (Fig. 6), it is expected that hydrogen will desorb from Pd at lower temperatures when at lower hydrogen pressures. The intensity of the α-PdH(111) diffraction peak decreases at 300 °C, however, it is still detectable up until 700 °C suggesting that small traces of the α-PdH phase is stable at such high temperatures under 100 kPa of hydrogen pressure. This also means that minute remains of the Pd thin film can still be detected following interdiffusion with the bulk Pd-Cu foil under these conditions. Similar to what is shown in Fig. 5(a), interdiffusion takes place between 350 and 600 °C as demonstrated by the movement of the α-PdH(111) diffraction peak to higher scattering angles to eventually merge with the Pd-rich Pd-Cu(111) diffraction peak.

The Pd-Cu(111) diffraction peak associated with the bulk Pd-Cu foil does not disappear during the VTXRD experiment indicating that the FCC phase remains stable throughout the entire temperature range. According to Fig. 1, for a composition of $Pd_{60}Cu_{40}$ wt% only the BCC phase is stable below 425 °C. This implies that 100 kPa of hydrogen pressure is insufficient in promoting the complete transformation of the FCC phase to the BCC phase during the VTXRD run.
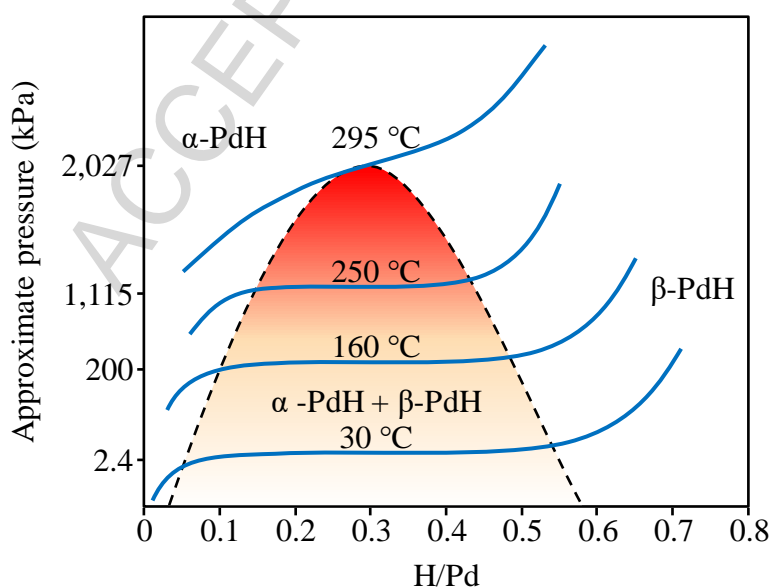

Fig. 6 Pd-H PCT diagram showing a series of isotherms that define the miscibility gap region.

12

The VTXRD results for Foils C2 and C3 are displayed in Fig. 7(a) and (b), respectively. Foil C2 readily forms the β-PdH phase at 30 °C under 445 kPa of hydrogen pressure as indicated by the β-PdH(111) diffraction peak positioned at 2θ = 38.41° as shown in Fig. 7(a). This scattering angle corresponds to a lattice parameter of 4.056 Å indicating a 13.4% Pd lattice volume expansion which is comparable to the 14.3% Pd lattice volume expansion experienced by Foil B2. Moreover, hydrogen desorption in Foil C2 occurs at the same temperature as Foil B2 (200 °C) forming the α-PdH phase as shown by the α-PdH(111) diffraction peak at 2θ = 39.81°.

At 400 °C, the α-PdH(111) diffraction peak moves to higher scattering angles to merge with the Pd-rich Pd-Cu(111) diffraction peak which appears above 400 °C. In addition, the Pd-Cu(111) diffraction peak associated with the bulk Pd-Cu foil disappears at 275 °C. In general, the Pd thin film seems to completely interdiffuse with the bulk Pd-Cu foil under the VTXRD conditions used.
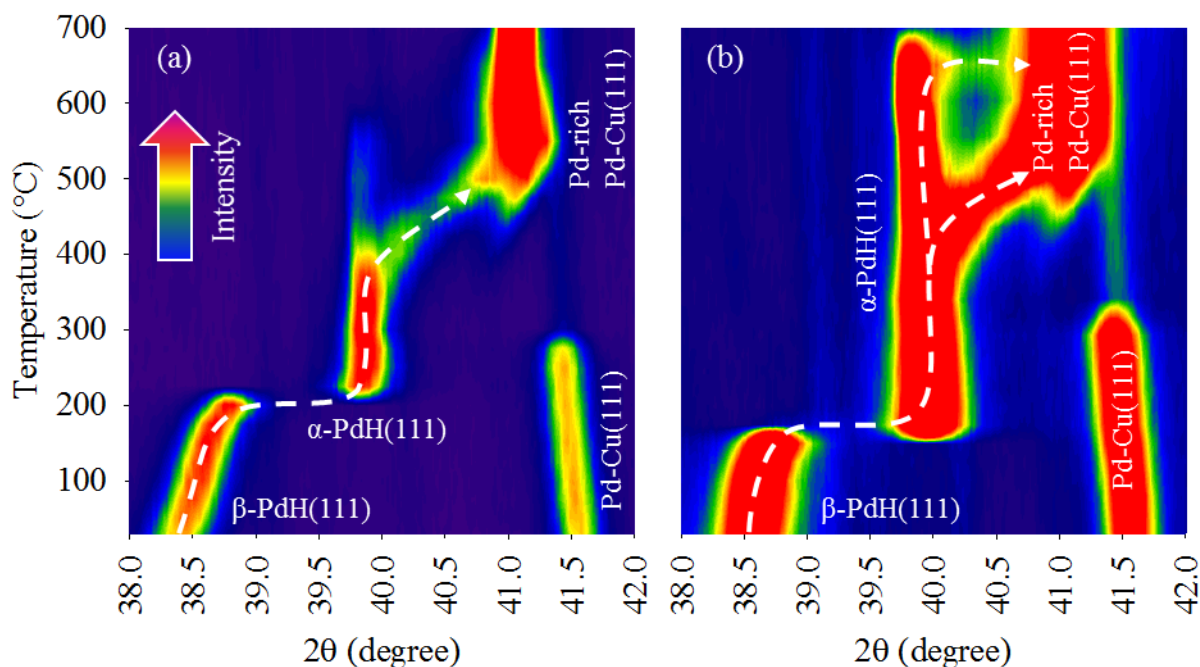

Fig. 7 VTXRD contour plots tracking the movement of the (a) PdH(111) diffraction peak from the Pd thin film of Foil C2 under 445 kPa of flowing hydrogen and (b) the PdH(111) diffraction peak from the Pd thin film of Foil C3 under 100 kPa of flowing hydrogen whilst heating between 30 and 700 °C.

For Foil C3, the β-PdH(111) diffraction peak appears at 2θ = 38.58° at a temperature of 30 °C and 100 kPa of hydrogen pressure as illustrated in Fig. 7(b). This corresponds to a lattice parameter of 4.039 Å which represents a 12.0% Pd lattice volume expansion. Hydrogen desorption from the Pd thin film occurs at 150 °C which is identical to the temperature at which hydrogen desorbs from the Pd thin film of Foil B3. This is represented by the movement of the β-PdH(111) diffraction peak to 2θ = 39.94° signalling the formation of the α-PdH phase which is indicated by the α-PdH(111) diffraction peak. This particular phase remains stable up to almost 700 °C. Under the VTXRD conditions, interdiffusion mainly occurs between 400 and 550 °C, ceases and then continues at 650 °C although the Pd thin film remains stable almost up to 700 °C. The Pd-Cu(111) diffraction peak originating

from the bulk Pd-Cu foil drops in intensity between 325 °C and merges with the
Pd-rich Pd-Cu(111) diffraction peak at 500 °C.

Fig. 8(a) and (b) show the VTXRD results for Foil D2 and Foil D3, respectively. As
evidenced in Fig. 8(a) by the β-PdH(111) diffraction peak at 2θ = 38.38°, Foil D2 readily
forms the β-PdH phase at 30 °C under 445 kPa of hydrogen pressure. A lattice parameter of
4.059 Å can be calculated from this scattering angle demonstrating that the Pd lattice volume
had expanded by 13.6%. This is similar to the lattice volume expansion observed for Foil B2
(14.3%) and Foil C2 (13.4%) at the same temperature and hydrogen pressure.
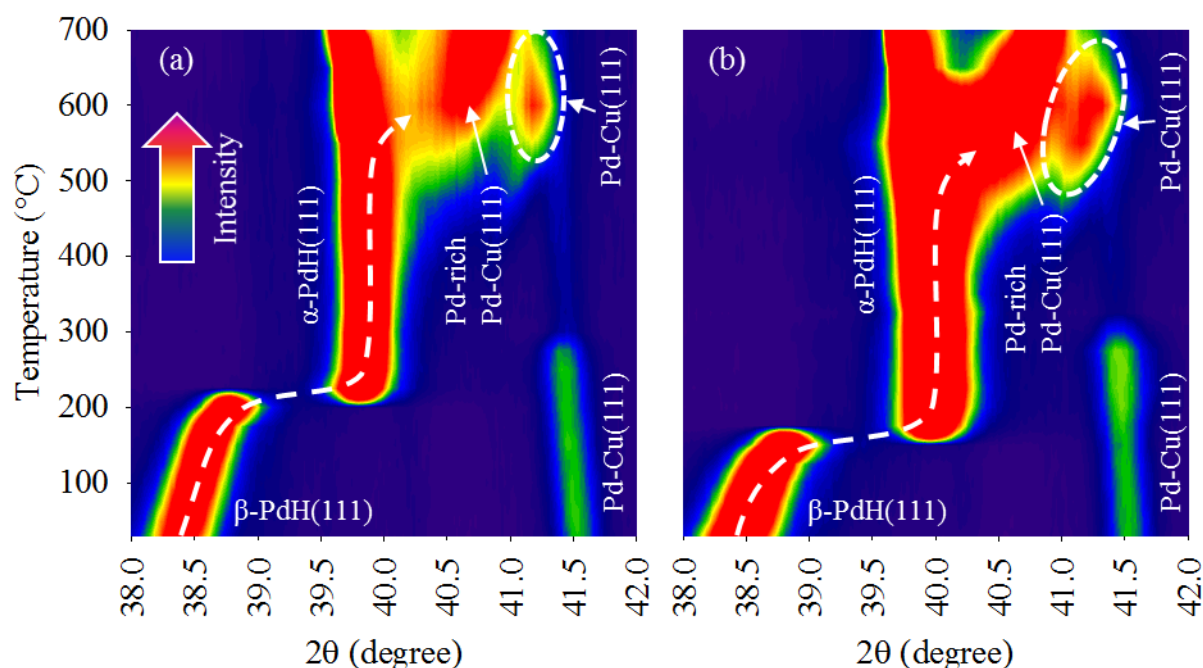

Fig. 8 VTXRD contour plots tracking the movement of the (a) PdH(111) diffraction peak from the Pd thin film of Foil D2 under 445 kPa of flowing hydrogen and (b) the PdH(111) diffraction peak from the Pd thin film of Foil D3 under 100 kPa of flowing hydrogen whilst heating between 30 and 700 °C.

Similar to Foils B2 and C2, hydrogen desorption from the Pd thin film in Foil D2
occurs at 200 °C in order to accommodate the β-PdH → α-PdH phase transformation. This is
indicated by the appearance of the α-PdH(111) diffraction peak at 2θ = 39.79°. Significant
interdiffusion takes place between 400 and 700 °C, however the α-PdH phase appears to be
stable even up to 700 °C meaning that the Pd thin film does not completely interdiffuse with
the bulk Pd-Cu foil under the conditions used in the VTXRD experiment. Furthermore, the
Pd-Cu(111) diffraction peak associated with the bulk Pd-Cu foil disappears at 300 °C and
reappears above 500 °C to merge with the Pd-rich Pd-Cu(111) diffraction peak at higher
temperatures.

At 30 °C and 100 kPa of hydrogen pressure, Fig. 8(b) reveals that in Foil D3 the
β-PdH(111) diffraction peak appears at 2θ = 38.45°. This scattering angle corresponds to a
lattice parameter of 4.052 Å representing a 13.0% Pd lattice volume expansion. Like in
Foils B3 and C3, the β-PdH → α-PdH phase transformation occurs at 150 °C in Foil D3 as
demonstrated by the formation of the α-PdH(111) diffraction peak at 2θ = 39.96°. Similar to
Foil D2, interdiffusion in Foil D3 takes place between 400 and 650 °C and the α-PdH phase
remains stable up until 700 °C showing that the Pd thin film does not fully interdiffuse with

14

the bulk Pd-Cu foil at a hydrogen pressure of 100 kPa. In addition, the Pd-Cu(111) diffraction peak originating from the bulk Pd-Cu foil disappears at 325 °C and reappears at 500 °C to finally merge with the Pd-rich Pd-Cu(111) diffraction peak.

3.3   Post-VTXRD foil characterisation

Following the VTXRD runs, XPS depth profile analysis was carried out on Foils B2 and B3 with the results shown in Fig. 9(a) and (b), respectively. It appears that the top few nanometres of Foil B2 contain a Pd-rich phase with a composition of $Pd_{90.2}Cu_{9.8}$ wt%. Similarly, the surface of Foil B3 has a composition of $Pd_{87.9}Cu_{12.1}$ wt%. Both indicate the presence of the Pd-rich Pd-Cu FCC phase observed in Fig. 5(a) and (b).

The results for the XPS depth profile analysis performed on Foils C2 and C3 following VTXRD analysis is displayed in Fig. 9(c) and (d), respectively. It is apparent that Foil C2 contains the Pd-rich Pd-Cu FCC phase on the Pd sputter-coated surface giving a composition of $Pd_{85.6}Cu_{14.4}$ wt%. Moreover, Foil C3 shows evidence of the Pd-rich Pd-Cu FCC phase with a composition of $Pd_{89.5}Cu_{10.5}$ wt%. The Pd-rich Pd-Cu FCC phase associated with Foil C2 has a relatively higher Cu concentration likely caused through an increased rate of interdiffusion facilitated by the relatively higher hydrogen pressure.

The XPS depth profile analysis data for Foils D2 and D3 is shown in Fig. 9(e) and (f), respectively. Fig. 9(e) shows that the Pd sputter-coated side of Foil D2 has a Pd-rich Pd-Cu FCC phase composition of $Pd_{79.7}Cu_{20.3}$ wt%. The Cu concentration immediately increases and stabilises at a depth of around 50 nm and then steadily increases over the analysis depth. Fig. 9(f) shows that the top surface of Foil D3 has a composition of $Pd_{76.1}Cu_{23.9}$ wt%. The Cu concentration experiences a slight dip at a depth of 50 nm after which the composition remains relatively constant across the analysis depth.

Interestingly, the Pd-rich Pd-Cu FCC phase compositions for Foils D2 and D3 have a higher Cu content compared to the Pd-rich Pd-Cu FCC phase present in Foils C2 ($Pd_{85.6}Cu_{14.4}$ wt%) and C3 ($Pd_{89.5}Cu_{10.5}$ wt%). This could be attributed to the existence of a larger Cu concentration gradient introduced by the relatively thicker Pd thin film (~1,400 nm) in Foils D2 and D3 creating a greater driving force for Cu interdiffusion into the Pd thin film.
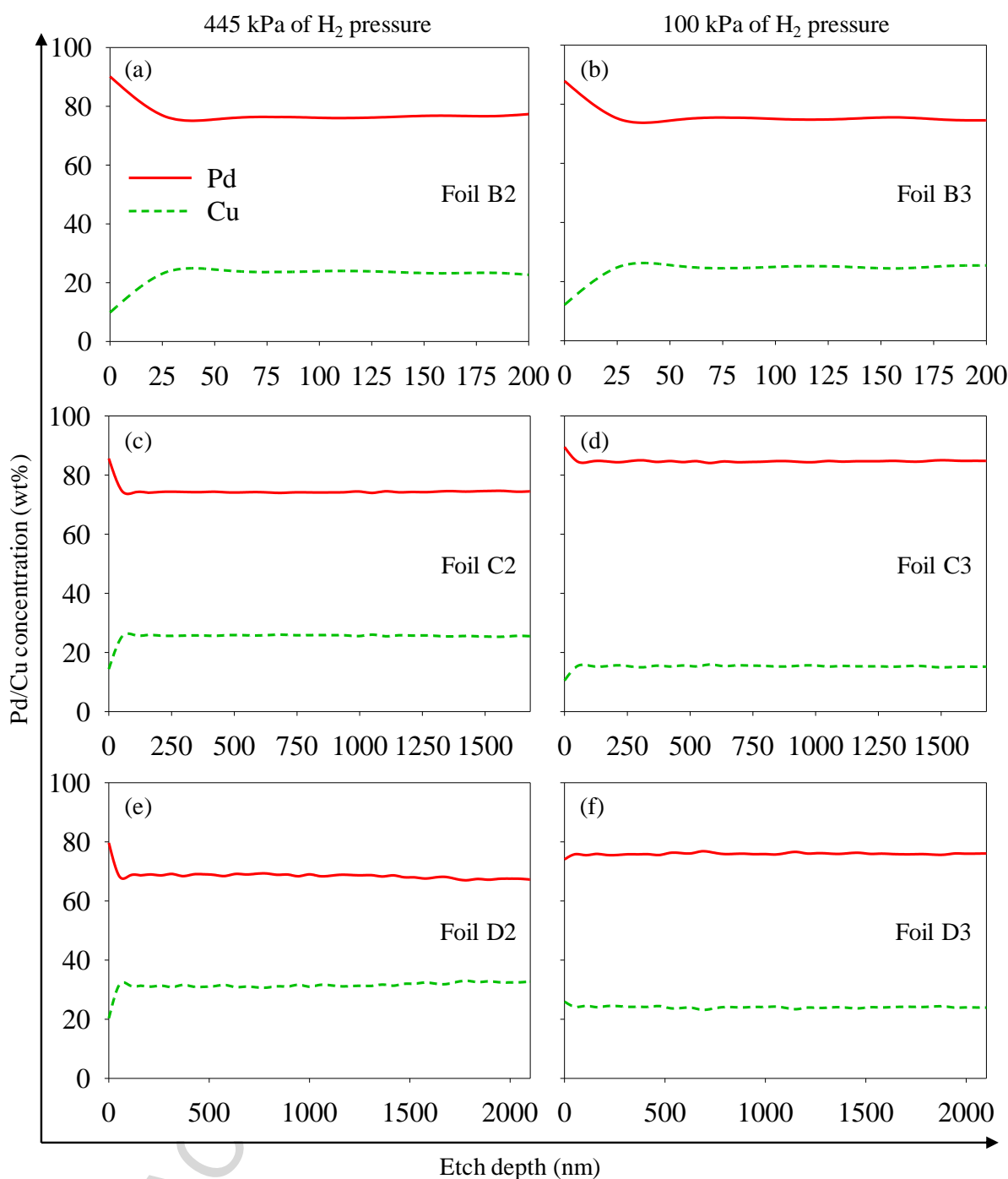
Fig. 9 XPS depth profile analysis of the Pd sputter-coated surface of (a) Foil B2, (b) Foil B3, (c) Foil C2, (d) Foil C3, (e) Foil D2 and (f) Foil D3 following VTXRD experiments.

3.4   General discussion

It is important to note that the thickness for the Pd thin film of the surface modified foil samples determined by XPS prior to VTXRD analyses is different from that measured via profilometry for two main reasons. Firstly, there is a difference in density between the Ta_2O_5 standard (8.18 g cm^{-3}), Pd (12.02 g cm^{-3}) and Pd-Cu foil (8.96 – 12.02 g cm^{-3}) meaning each would likely etch at different rates. Therefore, the thickness of the Pd thin film determined by profilometry is considered more accurate. Moreover, it has been shown that interdiffusion occurs between the Pd thin film and the bulk Pd-Cu foils during deposition. This has made it

16

difficult to determine where the Pd thin film ends and bulk Pd-Cu foil begins as there appears to be clear evidence of an interdiffusion region at the interface.

The effects of hydrogen on the Pd-Cu alloy system have become more apparent throughout the course of this study. Table 4 summarises the results obtained from the VTXRD study. At 445 kPa of hydrogen pressure, the β-PdH phase in Foils B2, C2 and D2 readily forms at 30 °C and is stable up until 225 °C. The hydrogen depleted α-PdH phase forms at 200 °C signalling that hydrogen desorption from the hydrogen rich β-PdH phase takes place.

It is evident that the α-PdH phase is stable to higher temperatures in the relatively thicker Pd thin film. For example, in Foil B2 the α-PdH phase remains present up until 450 °C, whereas in Foils C2 and D2 this phase disappears at 550 and 700 °C, respectively. This observation is plausible since a thicker Pd thin film which has a relatively larger amount of deposited Pd would require higher temperatures to completely interdiffuse with the bulk Pd-Cu foil compared with thinner films under same durations and VTXRD test conditions. The α-PdH phase present in Foils B2 and C2 disappear at 450 and 550 °C, respectively, likely due to the reduction in hydrogen solubility caused by an increase in Cu concentration in the Pd thin film [25].

At 100 kPa, the β-PdH phase forms between 30 and 150 °C in Foil B3, while in Foils C3 and D3 this phase is stable up to 175 °C. In the case of Foil B3, the β-PdH phase may exist up to 175 °C, however, since the β-PdH(111) diffraction peak reduces in intensity during the phase transformation to the α-PdH phase this peak becomes indistinguishable from the background noise.

The α-PdH phase is detected up to 700 °C in Foils B3, C3 and D3 (100 kPa of hydrogen pressure) which is higher than the temperatures observed for Foils B2, C2 and D2 (445 kPa of hydrogen pressure) indicating that at higher hydrogen pressures interdiffusion is accelerated. Furthermore, under 100 kPa of hydrogen pressure the Pd-Cu FCC phase originating from the as-received Pd-Cu foil offcut is stable over a wider temperature range compared with 445 kPa of hydrogen pressure. This can both be attributed to the formation of the well known vacancy-hydrogen clusters [42-45] that accelerate atomic diffusion responsible for rapid phase transformation and evidently increased rate of interdiffusion.

In Foils B2, B3, C2 and C3, interdiffusion occurs at the same temperatures. Although, in the case of Foils D2 and D3, this process starts at a higher temperature of 400 °C and potentially continues above 700 °C. This indicates that a portion of the Pd thin film in Foils D2 and D3 remains stable under the conditions used during the VTXRD experiment likely due to its relatively large thickness compared with the Pd thin films of Foils B2, B3, C2 and C3.

17

Table 4 Summary of the VTXRD results.

Surface modified foil samples	Hydrogen pressure (kPa)	β-PdH temperature range (°C)	α-PdH temperature range (°C)	Pd-Cu FCC temperature range (°C)	Interdiffusion temperature range (°C)
Foil B2	445	30 – 225	200 – 450	30 – 325, 500 – 700	350 – 600
Foil B3	100	30 – 150	150 – 700	30 – 700	350 – 600
Foil C2	445	30 – 225	200 – 550	30 – 275, 450 – 700	350 – 600
Foil C3	100	30 – 175	150 – 700	30 – 325, 450 – 700	350 – 600
Foil D2	445	30 – 225	200 – 700	30 – 275, 475 – 700	400 – 700+
Foil D3	100	30 – 175	150 – 700	30 – 300, 475 – 700	400 – 700+

4   Conclusions

It was revealed with the use of XRD and XPS depth profile analysis that interdiffusion between the Pd thin film and Pd-Cu foil substrate occurs in the surface modified foil samples during the Pd deposition process. Various authors [35-40] postulate that the polycrystalline nature of a deposited thin film introduces grain boundary defects through which interdiffusion can be facilitated at relatively low temperatures. Apparently, a Pd target current of 1 A is sufficient in producing temperatures necessary to allow interdiffusion between the Pd thin film and Pd-Cu foil substrate during deposition.

Furthermore, it has been shown using VTXRD analysis of the surface modified foil samples that the β-PdH phase is stable up to a maximum temperature of 175 °C under 100 kPa of hydrogen pressure. This limit is raised to 225 °C under 445 kPa of hydrogen pressure. The stability of the α-PdH phase depends on the thickness of the Pd thin film and hydrogen pressure. At 100 kPa of hydrogen pressure, the α-PdH phase remains stable up to 700 °C. Whereas, at 445 kPa of hydrogen pressure, the α-PdH phase disappears at 450 and 550 °C in Foils B2 and C2, respectively, as a result of a reduction in hydrogen solubility caused by Cu interdiffusion into the Pd thin film. It was also found that the Pd-Cu FCC phase attributed to the bulk Pd-Cu foil substrate is stable over a wider temperature range under 100 kPa of hydrogen pressure compared with 445 kPa of hydrogen pressure. This indicates that higher hydrogen pressures accelerate the Pd-Cu FCC to BCC phase transformation.

From this study, it can be surmised that parameters such as deposition conditions, thin film thickness, temperature and pressure are all paramount when designing surface modified dense metal membranes for hydrogen purification applications. In this case, it would appear that depositing a Pd thin film with a thickness greater than 1,400 nm onto a Pd-Cu foil substrate could yield a membrane material with a stable surface composition under typical operating conditions.

Acknowledgements

The authors are grateful to Johnson Matthey Noble Metals (Royston, UK) for the provision of rolled Pd-Cu foils and to NEXUS nanoLab (Newcastle University) for their help with the XPS analysis. The support from the EPSRC (United Kingdom) Doctoral Training Centre (DTC) in Hydrogen, Fuel Cells and their Applications (EP/G037116/1) is gratefully acknowledged, as is the support from the research group of Professor David Book, School of Metallurgy and Materials, University of Birmingham.

References

[1] L. Barelli, G. Bidini, F. Gallorini, S. Servili, Hydrogen production through sorption-enhanced steam methane reforming and membrane technology: A review, Energy, 33 (2008) 554-570.

[2] J.D. Holladay, J. Hu, D.L. King, Y. Wang, An overview of hydrogen production technologies, Catalysis Today, 139 (2009) 244-260.

[3] A. Faur Ghenciu, Review of fuel processing catalysts for hydrogen production in PEM fuel cell systems, Current Opinion in Solid State and Materials Science, 6 (2002) 389-399.

[4] A.G. Knapton, Palladium alloys for hydrogen diffusion membranes, Platinum Metals Review, 21 (1977) 44-50.

[5] S. Adhikari, S. Fernando, Hydrogen membrane separation techniques, Industry & Engineering Chemistry Research, 45 (2006) 875-881.

[6] S.N. Paglieri, J.D. Way, Innovations in palladium membrane research, Separation and Purification Methods, 31 (2002) 1-169.

[7] K. Zhang, J.D. Way, Palladium-copper membranes for hydrogen separation, Separation and Purification Technology, 186 (2017) 39-44.

[8] N. Al-Mufachi, N. Rees, R. Steinberger-Wilkens, Hydrogen selective membranes: A review of palladium-based dense metal membranes, Renewable and Sustainable Energy Reviews, 47 (2015) 540-551.

[9] D.L. McKinley, Metal alloy for hydrogen separation and purification, U.S. Patent 3,350,845 (1967).

[10] D.L. McKinley, Method for hydrogen separation and purification, U.S. Patent 3,439,474 (1969).

[11] K.S. Rotherberg, B.H. Howard, R.P. Killmeyer, M.V. Ciocco, B.D. Morreale, R.M. Enick, Palladium-copper alloy membrane performance under continuous exposure, in: National Hydrogen Association, Washington, DC, 2005, pp. 1-10.

[12] N. Pomerantz, Y.H. Ma, Effect of H_2S on the performance and long-term stability of Pd/Cu membranes, Industrial & Engineering Chemistry Research, 48 (2009) 4030-4039.

[13] N. Pomerantz, Y.H. Ma, Novel method for producing high H_2 permeability Pd membranes with a thin layer of the sulfur tolerant Pd/Cu fcc phase, Journal of Membrane Science, 370 (2011) 97-108.

[14] B. Morreale, M. Ciocco, B. Howard, R. Killmeyer, A. Cugini, R. Enick, Effect of hydrogen-sulfide on the hydrogen permeance of palladium–copper alloys at elevated temperatures, Journal of Membrane Science, 241 (2004) 219-224.

[15] P. Subramanian, D. Laughlin, Cu-Pd (copper-palladium), Journal of Phase Equilibria, 12 (1991) 231-243.

[16] J. Piper, Diffusion of hydrogen in copper-palladium alloys, Journal of Applied Physics, 37 (1966) 715-721.

[17] B. Howard, R. Killmeyer, K. Rothenberger, A. Cugini, B. Morreale, R. Enick, F. Bustamante, Hydrogen permeance of palladium–copper alloy membranes over a wide range of temperatures and pressures, Journal of Membrane Science, 241 (2004) 207-218.

[18] L. Yuan, A. Goldbach, H. Xu, Permeation hysteresis in PdCu membranes, Journal of Physical Chemistry B, 112 (2008) 12692-12695.

[19] N. Al-Mufachi, R. Steinberger-Wilckens, X-ray diffraction study on the effects of hydrogen on $Pd_{60}Cu_{40}$ wt% foil membranes, Journal of Membrane Science, 545 (2018) 266-274.

[20] M. Li, Z. Du, C. Guo, C. Li, A thermodynamic modeling of the Cu–Pd system, Calphad, 32 (2008) 439-446.

[21] J. Völkl, G. Alefeld, Diffusion of hydrogen in metals, in: G. Alefeld, J. Völkl (Eds.) Hydrogen in metals I, Springer, Berlin, 1978, pp. 321-348.

[22] P. Kamakoti, D.S. Sholl, A comparison of hydrogen diffusivities in Pd and CuPd alloys using density functional theory, Journal of Membrane Science, 225 (2003) 145-154.

[23] M.H. Martin, J. Galipaud, A. Tranchot, L. Roué, D. Guay, Measurements of hydrogen solubility in Cu_xPd_{100-x} thin films, Electrochimica Acta, 90 (2012) 615-622.

[24] T. Flanagan, D. Chisdes, Solubility of hydrogen (1 atm, 298 K) in some copper/palladium alloys, Solid State Communications, 16 (1975) 529-532.

[25] R. Burch, R. Buss, Absorption of hydrogen by palladium–copper alloys. Part 2.— Theoretical analysis, Journal of the Chemical Society, Faraday Transactions 1: Physical Chemistry in Condensed Phases, 71 (1975) 922-929.

[26] N. Al-Mufachi, S. Nayebossadri, J. Speight, W. Bujalski, R. Steinberger-Wilckens, D. Book, Effects of thin film Pd deposition on the hydrogen permeability of Pd 60 Cu 40 wt% alloy membranes, Journal of Membrane Science, 493 (2015) 580-588.

[27] K. Cooke, J. Hamsphire, W. Southall, D. Teer, The industrial application of pulsed DC bias power supplies in closed field unbalanced magnetron sputter ion plating, Surface and Coatings Technology, 177 (2004) 789-794.

[28] L. Vegard, Die konstitution der mischkristalle und die raumfüllung der atome, Zeitschrift für Physik A Hadrons and Nuclei, 5 (1921) 17-26.

[29] S. Nayebossadri, J. Speight, D. Book, Effects of low Ag additions on the hydrogen permeability of Pd–Cu–Ag hydrogen separation membranes, Journal of Membrane Science, 451 (2014) 216-225.

[30] L. Yuan, A. Goldbach, H. Xu, Segregation and H_2 transport rate control in body-centered cubic PdCu membranes, Journal of Physical Chemistry B, 111 (2007) 10952-10958.

[31] P.L. Gai, B.C. Smith, Dynamic electron microscopy of copper-palladium intermetallic compound catalysts, Ultramicroscopy, 34 (1990) 17-26.

[32] H. Gao, J.Y. S. Lin, Y. Li, B. Zhang, Electroless plating synthesis, characterization and permeation properties of Pd–Cu membranes supported on ZrO_2 modified porous stainless steel, Journal of Membrane Science, 265 (2005) 142-152.

[33] F. Roa, J.D. Way, The effect of air exposure on palladium–copper composite membranes, Applied Surface Science, 240 (2005) 85-104.

[34] R. Merkle, J. Maier, On the Tammann–Rule, Zeitschrift für Anorganische und Allgemeine Chemie, 631 (2005) 1163-1166.

[35] S. Nakahara, J.A. Abys, S.M. Abys, Room-temperature diffusion-induced grain boundary migration in the fine-grained Pd side of Cu-Pd diffusion couples, Materials Letters, 2 (1983) 155-159.

[36] Y. Kuru, M. Wohlschlögel, U. Welzel, E.J. Mittemeijer, Interdiffusion and stress development in Cu–Pd thin film diffusion couples, Thin Solid Films, 516 (2008) 7615-7626.

[37] J. Chakraborty, U. Welzel, E. Mittemeijer, Mechanisms of interdiffusion in Pd–Cu thin film diffusion couples, Thin Solid Films, 518 (2010) 2010-2020.

[38] J. Chakraborty, U. Welzel, E. Mittemeijer, Interdiffusion, phase formation, and stress development in Cu–Pd thin-film diffusion couples: Interface thermodynamics and mechanisms, Journal of Applied Physics, 103 (2008) 113512.

[39] A. Bukaluk, Influence of depth resolution on interdiffusion measurements in polycrystalline Cu/Pd multilayers, Surface and Interface Analysis, 30 (2000) 597-602.

[40] A. Bukaluk, AES studies of interdiffusion in thin-film copper–palladium multilayer structures, Vacuum, 54 (1999) 279-283.

[41] K. Buschow, P. Bouten, A. Miedema, Hydrides formed from intermetallic compounds of two transition metals: a special class of ternary alloys, Reports on Progress in Physics, 45 (1982) 937.

[42] E. Hayashi, Y. Kurokawa, Y. Fukai, Hydrogen-induced enhancement of interdiffusion in Cu-Ni diffusion couples, Physical Review Letters, 80 (1998) 5588-5590.

[43] N. Fukumuro, M. Yokota, S. Yae, H. Matsuda, Y. Fukai, Hydrogen-induced enhancement of atomic diffusion in electrodeposited Pd films, Journal of Alloys and Compounds, 580, Supplement 1 (2013) S55-S57.

[44] T.B. Flanagan, C.-N. Park, Hydrogen-induced rearrangements in Pd-rich alloys, Journal of Alloys and Compounds, 293 (1999) 161-168.

[45] Y. Fukai, Formation of superabundant vacancies in M–H alloys and some of its consequences: a review, Journal of Alloys and Compounds, 356 (2003) 263-269.

Highlights

- High H2 pressures can stabilise the palladium hydride phase to higher temperatures
- 445 kPa of H2 pressure stabilises the palladium hydride phase to 225 °C
- Cu interdiffusion occurs between the Pd-Cu foil and Pd thin film during deposition